IOPscience

HOME | SEARCH | PACS & MSC | JOURNALS | ABOUT | CONTACT US

On the Miller-indices determination of $Si_{\{100\}}$ convex corner undercut planes

This article has been downloaded from IOPscience. Please scroll down to see the full text article.

2005 J. Micromech. Microeng. 15 833

(http://iopscience.iop.org/0960-1317/15/4/022)

The Table of Contents and more related content is available

Download details:
IP Address: 140.112.113.225
The article was downloaded on 17/12/2008 at 09:30

Please note that terms and conditions apply.

INSTITUTE OF PHYSICS PUBLISHING JOURNAL OF MICROMECHANICS AND MICROENGINEERING

J. Micromech. Microeng. **15** (2005) 833–842 doi:10.1088/0960-1317/15/4/022

On the Miller-indices determination of $Si_{\{1\,0\,0\}}$ convex corner undercut planes

W T Chang Chien[1], C O Chang[2], Y C Lo[3], Z W Li[2] and C S Chou[2]

[1] Department of Information Management, Fooyin University, Ta-Liao, Kaohsiung Hsien, Taiwan, Republic of China

[2] Institute of Applied Mechanics, National Taiwan University, Taipei, Taiwan, Republic of China

[3] National Synchrotron Radiation Research Center, Science-Based Industrial Park, Hsin-Shi, Taiwan, Republic of China

Received 15 August 2004, in final form 28 January 2005
Published 11 March 2005
Online at stacks.iop.org/JMM/15/833

Abstract

The Miller-indices determination of the arising surfaces at the $Si_{(0\,0\,1)}$ convex corner due to anisotropic etching is investigated. We propose a 2D zoning model in which the undercut planes arising at a masked convex corner are presumed to be in the same zone as the sidewalls forming the convex corner, which is characterized by the parallelism of the intersection lines of each pair of new surfaces and the sidewalls. Based on this model a method combining the experimental data, analytical geometry and stereographic projection is presented to systematically determine the Miller indices of the arising planes. The quantitative prediction of undercut planes is confirmed by the angle measurement using a surface profiler.

(Some figures in this article are in colour only in the electronic version)

1. Introduction

Due to the rapid growth of the microelectromechanical system (MEMS) market the use of anisotropic wet etching of single crystals in MEMS processing has increased. Anisotropic etching is considered indispensable when certain planes inclined with the wafer surface, which cannot be fabricated by plasma dry etching, are needed. Also the increasing complexity of an MEMS device gives the impetus to the study of anisotropic etching for many unsolved problems. The study of the etch rates of silicon crystal planes can be found in the papers of Seidel *et al* [1], Herr and Baltes [2] and Zielke and Frühauf [3], also the etch rates of polycrystalline SiO_2 and Si_3N_4 can be found in [1, 4, 5]. Papers [6–9] investigated the etching behavior of silicon crystals. The undercutting behavior of convex corners was reported in [10–13]. Designs of compensating structures for avoiding the emergence of the undercut facets were depicted in [11, 14, 15]. The final shapes of etched crystals were analysed either by the method of Wulff-type construction [16, 17] which is based on the equilibrium thermodynamics, or by the kinematic wave theory [18]. Given etch rate diagrams, papers [19, 20] developed their own simulation programs to predict the etched shapes of crystals using some geometrical methods.

As to the anisotropic etching of a convex corner on {1 0 0} silicon with the mask edge parallel to the ⟨1 1 0⟩ direction, Mayer [12] claimed that the arising planes at the corner are the {4 1 1} ones as shown in figure 1. Schröder [13] proposed that the anisotropic etching is mainly a step flow mechanism, and predicted the direction of bunched step lines (as shown in figure 2(*a*)) on the arising planes (the area B in figure 2(*b*)) occurring at the convex corner. Schröder did not state definitely what the Miller indices of these arising planes are. Bean [6], using a KOH–water–propanol etch solution, identified these planes as the {3 3 1} planes, while Abu-Zeid [11], using ethylene diamine–water solution instead, claimed them as the {2 1 2} planes. If we look with care at the (1 0 0) stereographic projection diagram, it was found that Bean and Abu-Zeid marked the undercut planes and the {1 1 1} sidewalls on the same trace, while those undercut planes of Mayer were not located on the trace of the sidewalls. Lattice planes with stereographically projected points on the same trace means that the intersection lines of each pair of those planes are parallel; or in the generalized sense, when these lattice planes are moved passing through the origin, they will intersect at a

 © 2005 IOP Publishing Ltd Printed in the UK

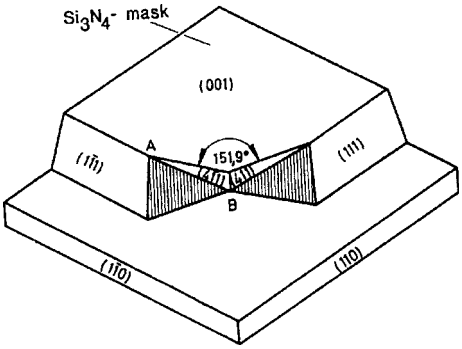

Figure 1. (4 1 1) planes occurring at convex corners during the KOH etching [12].

line. This line is called the zone axis of the zone in which those planes are situated. The important concept of being in the same zone for the undercut planes is that the orientations or Miller indices of those planes can be analysed and predicted by using 2D theory. Mayer determined the Miller indices of the undercut planes by an experimental technique. Neither Mayer nor Bean and Abu-Zeid provide a clear-cut method for identifying those undercut planes. We are engaged in this kind of study due to the fact that the method of properly determining the orientation of the undercut planes is insufficient and that the Miller-indices determination is indeed important in making the etch rate diagram of lattice planes.

In section 2 the etching solutions and the configurations of the $Si_{\{1\,0\,0\}}$ undercut convex corners are described. The 2D zoning of the undercut planes with the sidewalls of the convex corner are shown from the SEM micrographs. In section 3 the fundamental concepts and the necessary formula of crystallography are introduced. The evolution of the new surfaces arising at the convex corners in the process of anisotropic etching is explained step by step in section 4. A method, based on the proposed 2D zoning model and combining the analytical geometry, stereographic projection [21–23] and the auxiliary tool of the Wulff net, is presented in section 5 for the Miller-indices determination of the arising planes. A surface profiler is used to measure the angle between the undercut plane and the mask surface to verify the theoretically obtained result. This consistency proves the 2D zoning model which states that the undercut planes (area B in figure 2(*b*)) are in the same zone as the sidewalls.

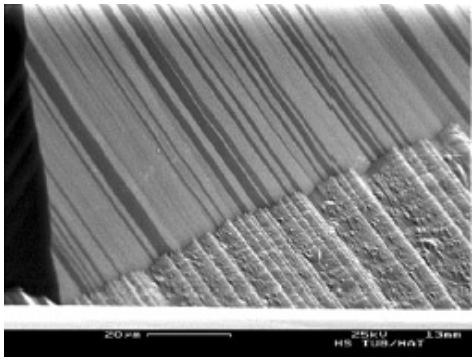

(*a*)

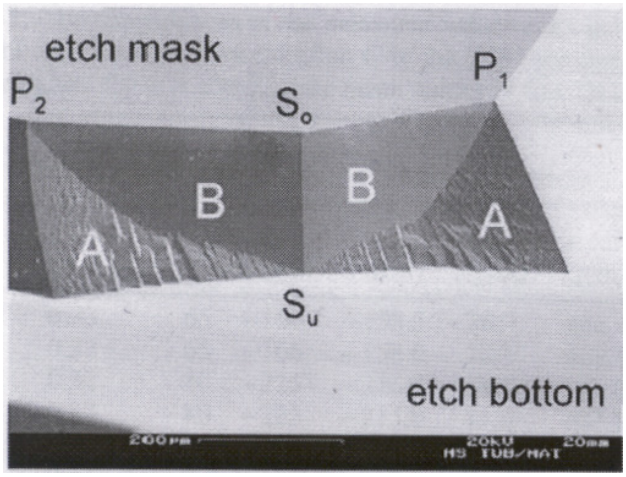

(*b*)

Figure 2. (*a*) SEM micrograph of coarse bunched step lines at area B occurring at convex corner undercut planes during the KOH etching [13]. (*b*) Undercut planes B occurring at convex corners.

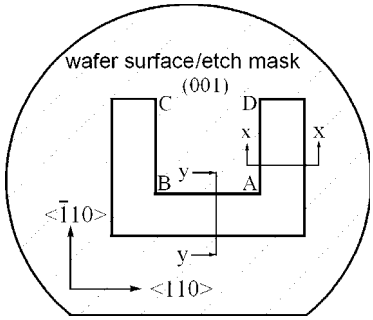

Figure 3. Mask pattern for the undercut etching.

2. Convex corner etching

p-type {1 0 0} oriented silicon wafers were etched in aqueous KOH solutions. Two different concentrations of KOH were used, one is KOH:H_2O = 3 : 7 and the temperature is maintained at $70 \pm 1\,^{\circ}$C, the other is KOH:H_2O = 4 : 6 and the temperature is maintained at $80 \pm 1\,^{\circ}$C. The mask pattern is shown in figure 3. After 10 min etching using KOH of 30% the convex corner A of figure 3 was photographed by SEM as shown in figure 4. For this short-period etching only a pair of symmetric undercut planes appears, these two planes are identified as of the {7 7 2} family instead of {4 1 1} reported by Mayer and will be explained later on. It is clear from this graph that the intersection lines of the undercut planes (7 $\bar{2}$ 7) and (7 2 7), (7 $\bar{2}$ 7) and the sidewall (1 $\bar{1}$ 1), and (7 2 7) and (1 1 1), are indeed parallel; this parallelism is evidence for the undercut planes to be in the same zone as the {1 1 1} sidewalls. Figure 5 shows the configuration of the etched convex corner after 50 min etching with KOH of 30%. The undercut structures after 100 min etching with 40% KOH are shown in figure 6. We find that both cases produce the same undercut structure as those obtained previously by Mayer and Schröder. The symmetric undercut planes are again identified, by our proposed method, as of the {7 7 2} family. Besides these, there exist two additional rough undercut surfaces marked as *S*.

In the other two etching experiments the same mask opening is used but the etching solutions are replaced by

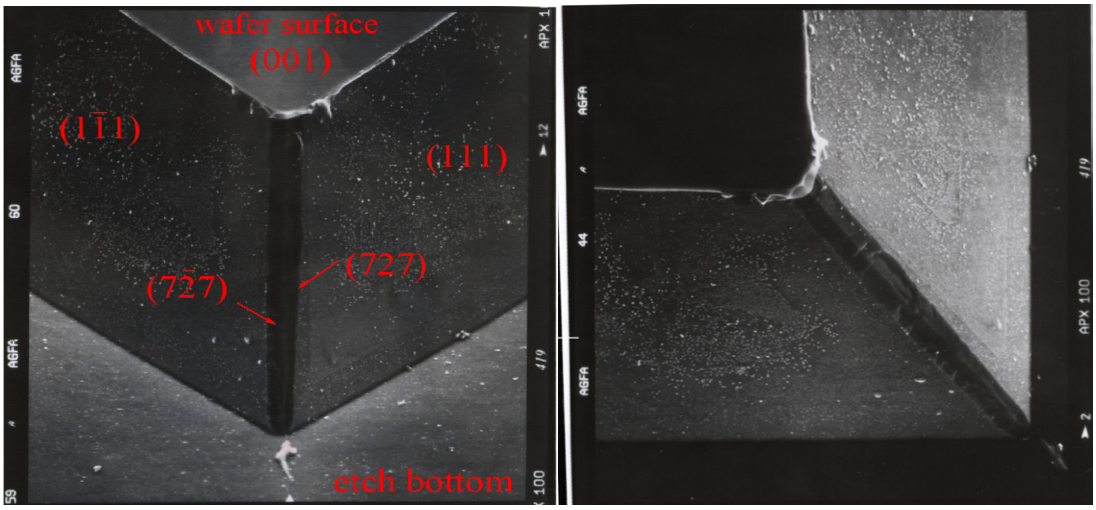

Figure 4. The SEM micrograph of the convex corner A marked in figure 3 shows the onset of the emerging new undercut planes, which were etched with 30% KOH at 70 °C.

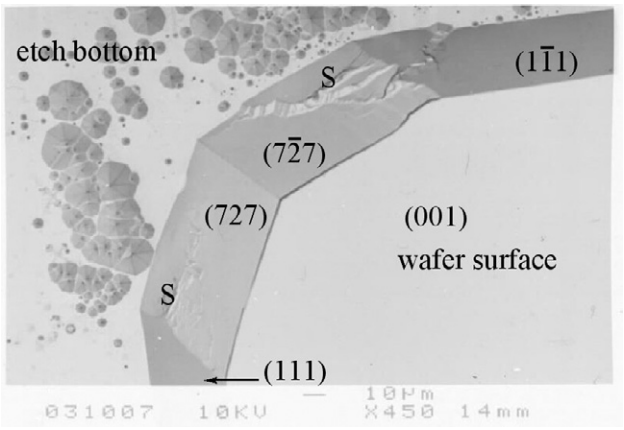

Figure 5. The SEM micrograph shows the configuration of the convex corner A marked in figure 3, which was etched with KOH of 30% and 50 min etching time at 70 °C. Except for the symmetric (7 2 7) and (7 $\bar{2}$ 7) undercut planes, another pair of undercut surfaces marked as *S* appears.

KOH + IPA. In one experiment KOH:H_2O = 3 : 7 and temperature is kept at 70 ± 1 °C, in the other KOH:H_2O = 4 : 6 and temperature is kept at 80 ± 1 °C. It is found that, although the concentration and temperature are different, they produce the same undercut planes as shown in figure 7.

3. Fundamental theory

Since we propose to use a combination of analytical geometry and the stereographic projection to determine the Miller indices of undercut planes, certain concepts of crystallography must be introduced in advance. In this section we will introduce the necessary condition for a lattice plane to be in the same zone as the other two lattice planes. A powerful technique for determining the Miller indices of a lattice plane, with known orientation, directly from the stereogram is described and will be used in the following sections.

The Miller indices $(h\,k\,l)$ of a lattice plane mean that this plane makes the intercepts a/h, b/k, c/l on the orthogonal x, y, z axes, respectively. The equation describing this plane in terms of the lattice parameters a, b, c of a unit cell is

$$\frac{x}{a/h} + \frac{y}{b/k} + \frac{z}{c/l} = 1,$$

or

$$f(x, y, z) = \frac{hx}{a} + \frac{ky}{b} + \frac{lz}{c} - 1 = 0. \tag{1}$$

The unit normal vector of this plane is

$$\mathbf{n} = \frac{\nabla f}{|\nabla f|} = \frac{1}{\sqrt{(h/a)^2 + (k/b)^2 + (l/c)^2}} \left(\frac{h}{a}\frac{k}{b}\frac{l}{c}\right)^{\mathrm{T}}. \tag{2}$$

The superscript 'T' means the transport operator and ∇ represents the gradient operator. For a cubic system we have $a = b = c$, then $\mathbf{n} = (h\,k\,l)^{\mathrm{T}}/\sqrt{h^2 + k^2 + l^2}$; it is obvious that $\mathbf{n}$ is parallel to the direction $[h\,k\,l]$. So the Miller indices of a lattice plane can also represent the components of its normal vector for cubic crystals.

3.1. Zone and zone axis

Any two non-parallel lattice planes $(h_1\,k_1\,l_1)$ and $(h_2\,k_2\,l_2)$ intersect at a line. Let their normal vectors be $\mathbf{n}_1 = (h_1\,k_1\,l_1)^{\mathrm{T}}$ and $\mathbf{n}_2 = (h_2\,k_2\,l_2)^{\mathrm{T}}$, then the intersection line is represented by the vector

$$\mathbf{L} = \mathbf{n}_1 \times \mathbf{n}_2 = (uvw)^{\mathrm{T}}, \tag{3}$$

where

$$u = k_1l_2 - l_1k_2, \quad v = l_1h_2 - h_1l_2 \quad \text{and} \quad w = h_1k_2 - k_1h_2.$$

The line represented by $\mathbf{L}$ is said to be the zone axis of the zone in which the two planes $(h_1\,k_1\,l_1)$ and $(h_2\,k_2\,l_2)$ are situated. The condition for the third plane $(h_3\,k_3\,l_3)$ to be of this zone $\langle uvw\rangle$ is that

$$\mathbf{n}_3 \cdot \mathbf{L} = \mathbf{0}, \qquad \text{or} \qquad h_3u + k_3v + l_3w = 0, \tag{4}$$

where $\mathbf{n}_3 = (h_3\,k_3\,l_3)^{\mathrm{T}}$.

The two undercut planes in figure 4 will be identified as (7 2 7) and (7 $\bar{2}$ 7) planes in section 4. We will see that the intersection line $\mathbf{L}_1$ of (7 2 7) and the sidewall (1 1 1), and the

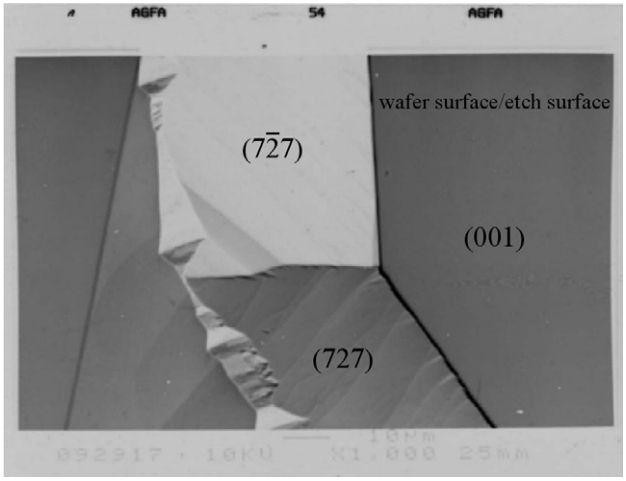

(*a*)

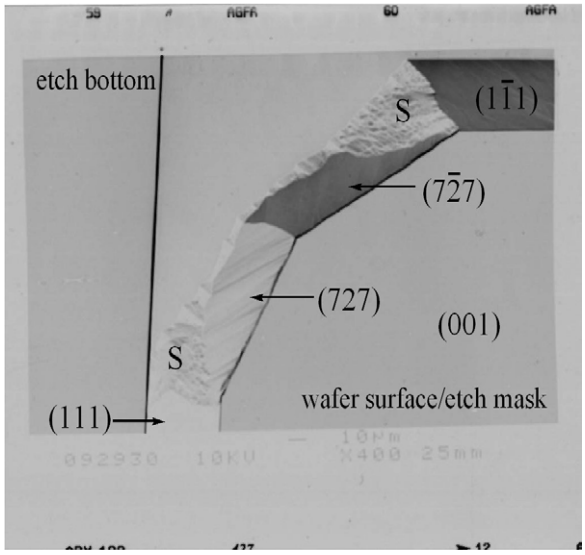

(*b*)

Figure 6. (*a*) The SEM micrograph of the convex corner A marked in figure 3 shows the undercut structures, which were etched with 40% KOH and 100 min etching time at 70 °C. (*b*) For this long-period etching, except for the symmetric (7 2 7) and (7 $\bar{2}$ 7) undercut planes, another pair of undercut surfaces marked as *S* appears.

intersection line $\mathbf{L}_2$ of (7 $\bar{2}$ 7) and (1 $\bar{1}$ 1), are parallel because

$$\vec{L}_1 = \begin{vmatrix} \vec{i} & \vec{j} & \vec{k} \\ 7 & 2 & 7 \\ 1 & 1 & 1 \end{vmatrix} = -5\vec{i} + 5\vec{k},$$

$$\vec{L}_2 = \begin{vmatrix} \vec{i} & \vec{j} & \vec{k} \\ 1 & -1 & 1 \\ 7 & -2 & 7 \end{vmatrix} = -5\vec{i} + 5\vec{k},$$

and the zone axis of the two sidewalls (1 $\bar{1}$ 1) and (1 1 1) is

$$\vec{L} = u\vec{i} + v\vec{j} + w\vec{k} = \begin{vmatrix} \vec{i} & \vec{j} & \vec{k} \\ 1 & -1 & 1 \\ 1 & 1 & 1 \end{vmatrix} = -2\vec{i} + 2\vec{k},$$

therefore, we have $\vec{L}_1 \| \vec{L}$, $\vec{L}_2 \| \vec{L}$ and $\vec{L}_1 \| \vec{L}_2$. This parallelism indicates that the undercut planes are in the same zone as the sidewalls of the convex corner. These parallel lines $\vec{L}_1$ and $\vec{L}_2$ can be observed directly from figure 4. It is also easy to check that the condition given by equation (4) is satisfied by undercut plane (7 2 7) or (7 $\bar{2}$ 7) and the zone axis $\langle \bar{2}\,0\,2 \rangle$.

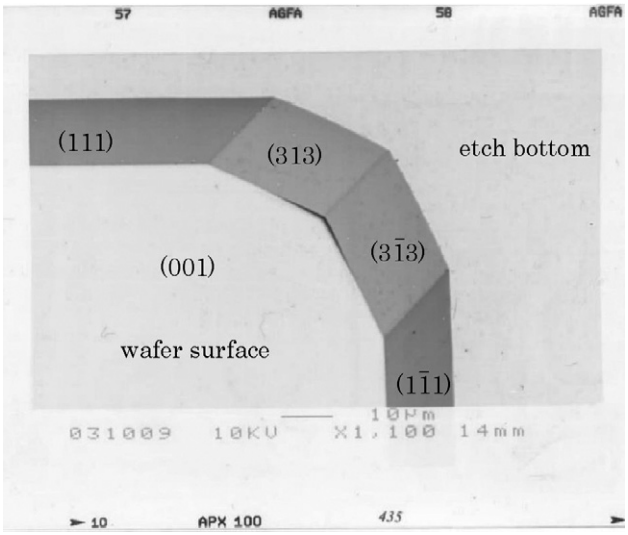

Figure 7. The SEM micrograph shows the configuration of the convex corner A marked in figure 3, which was etched with KOH+IPA of 40% and 60 min etching time at 70 °C.

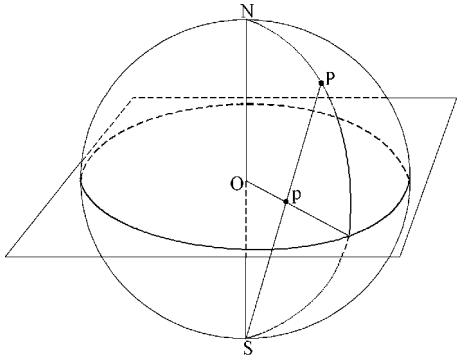

Figure 8. The stereographic projection p of a pole P in the northern hemisphere projected from the south pole.

3.2. Stereographic projection

Stereographic projection provides a means of representing the angular relationship in two dimensions, which will facilitate the measurement or discussion of the angles between crystal faces on a flat piece of paper. Imagine the crystal to be positioned with its center at the center of the sphere of projection and draw normals to crystal planes through the center of the sphere to intersect the surface of the sphere at point *P*. *P* is called the pole of the plane. A crystal plane can also be represented by drawing the parallel plane through the center of the sphere and extending it until it strikes the sphere. The line of intersection of the sphere with such a plane is called a great circle with radius equal to the radius of the sphere. We now project the point *P* on the sphere on to a flat piece of paper. Referring to figure 8, if we project the point *P* from the south point S on the sphere on to the equatorial plane normal to *SO*, the point p so produced on the equatorial plane is defined as the stereographic projection of *P*.

There are two important things coming from the stereographic projection. One is that angles on the sphere of

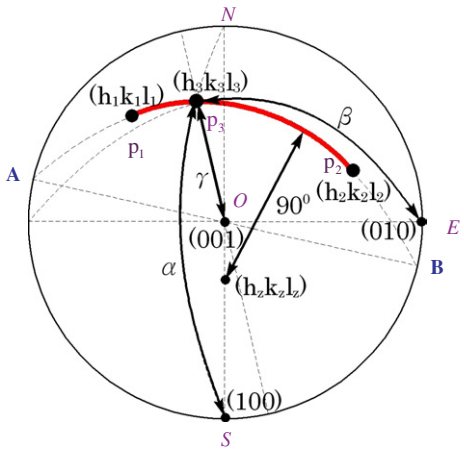

Figure 9. A stereogram illustrates the stereographic projection of crystal planes. Poles of planes $(h_1\,k_1\,l_1)$, $(h_2\,k_2\,l_2)$ and $(h_3\,k_3\,l_3)$ are on the circular trace $\widehat{AB}$, because they are in the same zone.

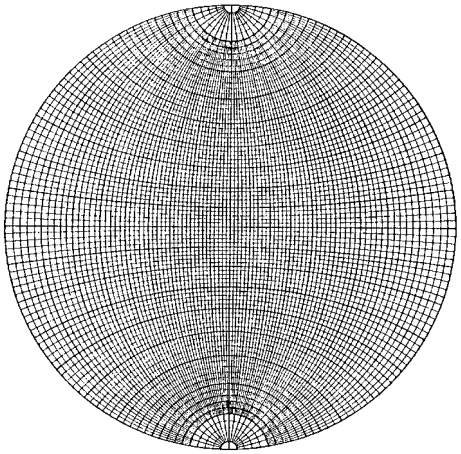

Figure 10. The Wulff net drawn at 2° intervals.

projection project as equal angles. The other is that all circles (great or small) on the surface of the sphere of projection project as circles. Let P_1 and P_2 be the poles on the sphere of projection of the two sidewalls $(h_1\,k_1\,l_1)$ and $(h_2\,k_2\,l_2)$ of a convex corner. Through these two poles we can draw a great circle. The circular arc AB in figure 9 is the partial stereographic projection of this great circle and is also called the trace of that great circle. $p_1$and p_2 are the corresponding stereographically projected poles. Now if the undercut plane $(h_3\,k_3\,l_3)$ is in the same zone of the sidewalls, from the above discussion, the pole p_3 of the stereographic projection of the undercut plane must lie on the same trace $\widehat{AB}$. With this concept in mind we will save a lot of effort in finding the Miller indices of the undercut planes. A Wulff net is a graphical aid for the construction of a stereogram. This net shown in figure 10 is drawn at 2° intervals. The net is used by placing it under the stereogram with two centers pinned together. The angle between poles is measured by rotating the stereogram until the two poles lie on the same great circle.

3.3. Miller indices measured from a stereogram

Now we turn to the problem of finding the Miller indices of a crystal plane with its orientations known. Referring to

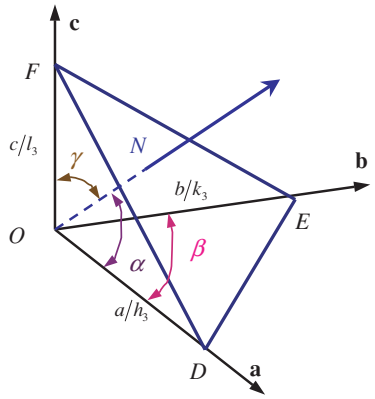

Figure 11. Orientation of a crystal plane of the Miller indices $(h\,k\,l)$.

figure 11, the angles between the normal line of the crystal plane $(h_3\,k_3\,l_3)$and the orthogonal axes x, y and z are denoted respectively by α, β and γ. The Miller indices of this plane can be determined when the position of the stereographically projected pole in the stereogram is known. The angles α, β, γ shown in figure 11 can be obtained directly by measuring the angles between the poles p_3 and $S(1\,0\,0)$, poles p_3 and $E(0\,1\,0)$, and poles p_3 and $O(0\,0\,1)$, respectively, in figure 9 with the auxiliary Wulff net. From the right triangles ΔDON we have

$$\cos\alpha = \cos\angle NOD = \frac{ON}{OD} = \frac{ON}{a/h_3},$$

thus

$$h_3 = \frac{a}{ON}\cos\alpha. \tag{5}$$

Similarly, fromΔEON and ΔFON, we get

$$k_3 = \frac{b}{ON}\cos\beta, \qquad l_3 = \frac{c}{ON}\cos\gamma. \tag{6}$$

Combining equations (5) and (6) gives

$$h_3 : k_3 : l_3 = a\cos\alpha : b\cos\beta : c\cos\gamma. \tag{7}$$

For a cubic system we have $a = b = c$, then equation (7) reduces to

$$h_3 : k_3 : l_3 = \cos\alpha : \cos\beta : \cos\gamma, \tag{8}$$

that is, the ratio of Miller indices is the ratio of the directional cosines.

4. Etching behavior

In this section the mechanism of the emergence of the undercut planes is explained.

Figures 12(*a*) and (*b*) are the X–X and Y–Y cross sections of the mask opening given in figure 3. In the first period of etching the (1 0 0) substrate was etched down along the $\langle 0\,0\,\bar{1}\rangle$ direction as shown in figure 13. In the second period of etching the substrate was etched out continuously and at the concave corners a_1 and b_1, e_1, and f_1 (marked in figure 13) the {1 1 1} planes illustrated in figure 14 emerged. So the convex corner A of figure 3 was formed by the two {1 1 1} side planes which intersect at the edge $\overline{r_1r_2}$ as shown in figure 15. For this convex-corner configuration there are three

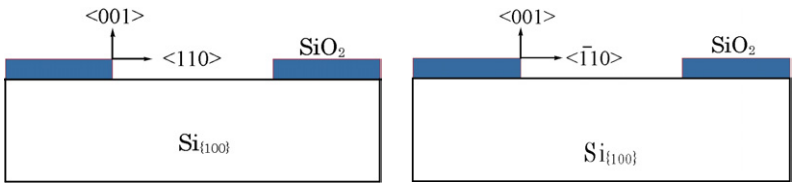

(*a*) **X-X cross section** (*b*) **Y-Y cross section**

Figure 12. The X–X and Y–Y cross sections of the masked opening given in figure 3.

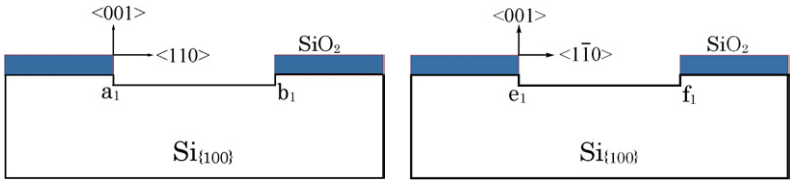

Figure 13. Etched structures of the X–X and Y–Y cross sections in the first period of etching.

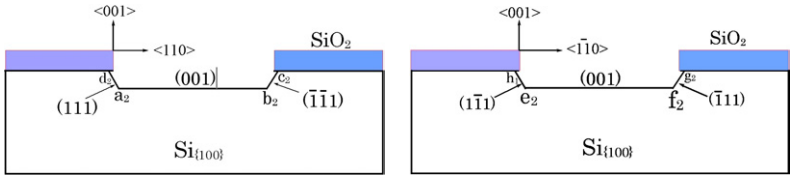

(*a*) **X-X cross section** (*b*) **Y-Y cross section**

Figure 14. Etched structures of the X–X and Y–Y cross sections in the second period of etching.

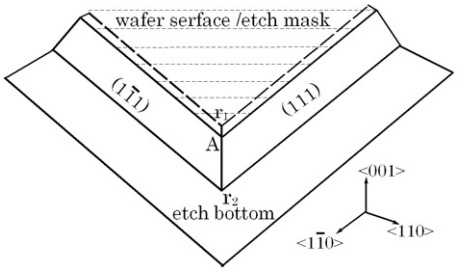

Figure 15. Configuration of corner A in the second period of etching.

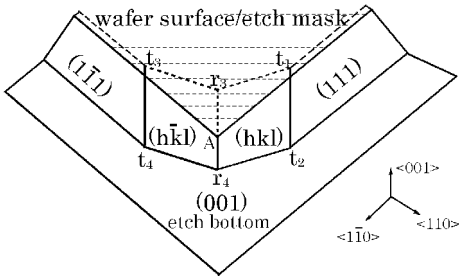

Figure 16. Undercutting occurring at corner A in the third period of etching.

regions where undercutting may occur: (1) the convex corner of the edge $\overline{r_1 r_2}$, (2) the region in the vicinity of point r_1, and (3) the region in the vicinity of point r_2.

According to the Séquin theorem [18] (based on kinematic wave theory) and the Wulff–Jacodine theorems [19] (based on equilibrium thermodynamic theory), we know that a convex corner remains convex after etching no matter how many new crystal planes appear; similarly, a concave corner keeps its concave shape after etching even if new crystal planes emerge. Furthermore, the new crystal planes at the convex corner are dominated by the faster-etching-rate planes, whereas the new planes occurring at the concave corner are dominated by the slower-etching-rate planes.

Now we consider the first case. The two sidewalls {1 1 1}, which form the convex corner of edge $\overline{r_1 r_2}$, have the slowest etch rates, some crystal planes with etch rates faster than these rates may occur, but only those of the fastest etch rates can emerge. The configuration of undercutting is shown in figure 16. Since the silicon single crystal belongs to the $m3m$ point group [24], if one undercut plane is $(h\,k\,l)$, due to the symmetry the crystal plane $(h\,\bar{k}\,l)$ also appears. Whether these two undercut planes are in the same zone as the sidewalls depends on whether the sectional lines $\overleftrightarrow{t_1 t_2}$ and $\overleftrightarrow{t_3 t_4}$ are parallel or not. The $(h\,k\,l)$ plane and the (0 0 1) substrate form a local concave corner. According to the above-mentioned theorem, this concave corner must remain concave even if undercutting occurs. If there exist some crystal planes whose etch rates are slower than $(h\,k\,l)$ and whose poles in the stereogram lie inside the sector formed by the origin and the poles of $(h\,k\,l)$ and (0 0 1), these new planes will emerge in the final period of etching and are represented by the concave-corner undercut planes S illustrated in figure 17.

Next we consider the second case. In the vicinity of point r_1 the (0 0 1) mask and the {1 1 1} sidewall form a concave corner; and the two {1 1 1} sidewalls form a convex corner. The etch rate of the SiO_2 mask approaches zero, and that of the {1 1 1} side wall is the slowest one of the silicon crystal, so there is no crystal plane with an etch rate slower. Therefore,

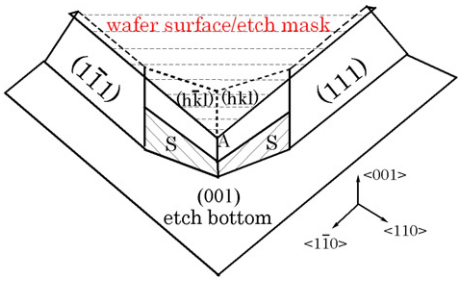

Figure 17. The new surfaces S emerge at the corner formed by the $\{h\,k\,l\}$ planes and the (0 0 1) substrate in the vicinity of corner A in the final period of etching.

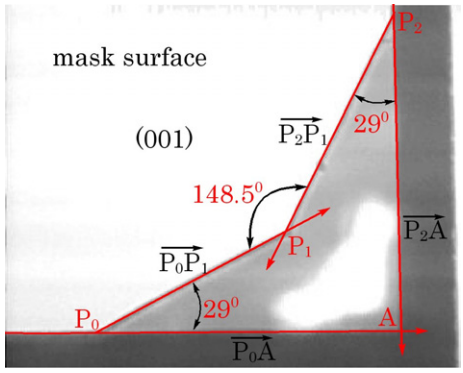

Figure 18. Top view of the microscope micrograph showing the mutual intersection lines of side walls, undercut planes and mask layer (KOH of 40%, temperature 70 °C, and 1 h etching time.)

it is not possible for the occurrence of new planes at this concave corner. But some crystal planes of faster etch rate may appear in the convex corner of edge $\overline{r_1r_2}$, this mechanism of undercutting belongs to that of the first case.

Finally we consider the third case, the corner in the vicinity of point r_2. The {1 1 1} side wall and the substrate (0 0 1) form a concave corner. Although there is no crystal plane having a slower etch rate than the {1 1 1} one, there may exist planes whose etch rates are slower than the (0 0 1); these planes have to compete for emergence with those $\{h\,k\,l\}$ planes arising at the convex corner of edge $\overline{r_1r_2}$ in the vicinity of point r_2. According to the rule that the fastest-etch-rate plane appears first at the convex corner, and that the slowest-etch-rate one occur first at the concave corner, it naturally leads to the conclusion that the slower-etch-rate plane appearing at the concave corner formed by a {1 1 1} and a (0 0 1) is predominated by the faster-etch-rate plane occuring at the convex corner formed by the two {1 1 1} plane of edge $\overline{r_1r_2}$. Indeed we do not observe any undercut plane at the concave corner at the point r_2 in our experiments. From the above discussion of the three possible undercutting cases, only the first one, that is, the undercutting at the convex corner of edge $\overline{r_1r_2}$, occurs. Based on these explanations, and the parallel character of the intersection lines of the undercut planes and the sidewalls shown in figures 4 and 7, we introduce a 2D zoning model to emphasize that the undercut planes near the mask layer should be formed in such a way that they are in the same zone as the sidewalls.

5. Miller indices of undercut planes

We first assume that the undercut planes are in the same zone as the sidewalls, based on this we determine the Miller indices of the undercut planes through measurement and the auxiliary tools of stereographic projection and Wulff net. The so-determined undercut planes are verified by experimental angle measurement using the surface profiler.

5.1. Aqueous KOH solutions

Referring to figure 18, which is the microscopic top-view graph, the vector $\overrightarrow{P_0A}$ coincides with the intersection line of the mask layer and the (1 $\bar{1}$ 1) sidewall, while vector $\overrightarrow{P_0P_1}$ coincides with that of the mask layer and the undercut plane of Miller indices $(h\,\bar{k}\,l)$. The angle between $\overrightarrow{P_0A}$ and $\overrightarrow{P_0P_1}$ is measured to be 29°. The projections of the directions $\langle 1\,\bar{1}\,1\rangle$ and $\langle h\,\bar{k}\,l\rangle$ on the (0 0 1) plane are $\langle 1\,\bar{1}\,0\rangle$ and $\langle h\,\bar{k}\,0\rangle$,

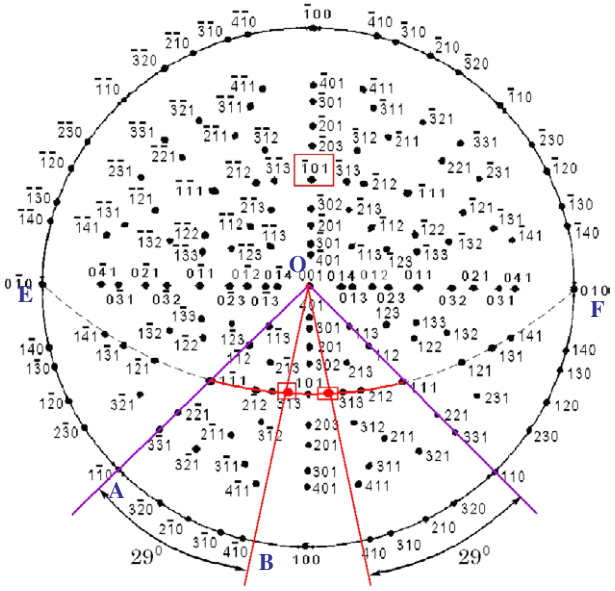

Figure 19. Location of the Miller indices of the undercut plane in ⟨0 0 1⟩ stereogram.

respectively; while $\langle 1\,\bar{1}\,0\rangle$ is the normal direction of the (1 $\bar{1}$ 0) plane and its pole in the stereogram is marked by the letter A in figure 19 and $\langle h\,\bar{k}\,0\rangle$ is the normal direction of the $(h\,\bar{k}\,0)$ plane and its pole is labeled by B. It is easy to show that the angle $\angle P_1P_0A$ is equal to the angle between the two planes (1 $\bar{1}$ 0) and $(h\,\bar{k}\,0)$. If we properly draw the line $\overleftrightarrow{OB}$ (where point O represents the pole of the (0 0 1) plane) at an angle 29° with respect to the line $\overleftrightarrow{OA}$ in figure 19, then the intersecting point of $\overleftrightarrow{OB}$ and the trace $\widehat{EF}$ of the two {1 1 1} sidewalls will be the projected pole of the $(h\,\bar{k}\,l)$ undercut plane.

Equation (8) given in section 3 will be used to calculate the Miller indices of the undercut planes. We first measure the angles α, β, γ of the direction $\langle h\,\bar{k}\,l\rangle$ with respect to the three axes $\langle 1\,0\,0\rangle$, $\langle 0\,\bar{1}\,0\rangle$ and $\langle 0\,0\,1\rangle$. It is found that $\alpha = 45°$, $\beta = 80°$ and $\gamma = 45°$. Then equation (8) gives $(h\,\bar{k}\,l) = (7\,\bar{2}\,7)$.

The above-mentioned method for the Miller-index determination is hands-on and systematic. An alternative which is purely a mathematical calculation is also presented here.

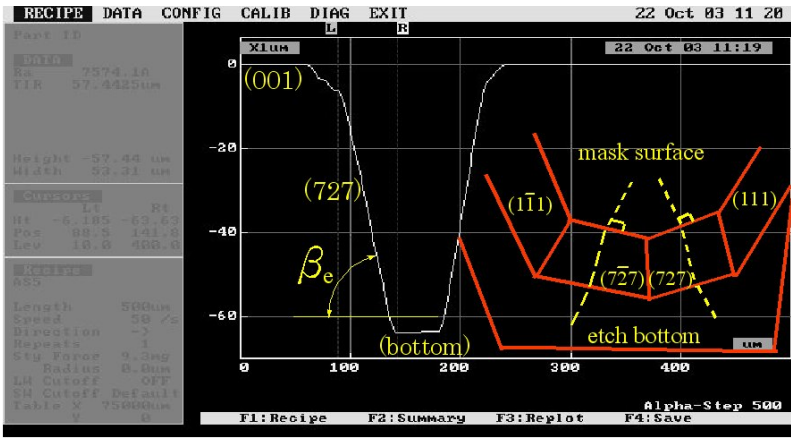

Figure 20. The inclination angle β_e of the (7 2 7) undercut plane with respect to the (0 0 1) plane measured by the surface profiler (Alpha-step) is 47.13°.

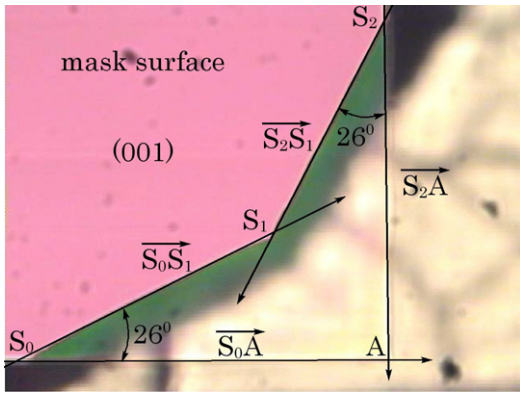

Figure 21. Top view of the microscope micrograph showing the mutual intersection lines of side walls, undercut planes and mask layer (KOH+IPA of 40%, temperature 70 °C and 100 min etching time.)

The component form of vector $\overrightarrow{P_0A}$ is

$$\overrightarrow{P_0A} = \langle 0\,0\,1\rangle \times \langle 1\,\bar{1}\,1\rangle = \begin{vmatrix} \vec{i} & \vec{j} & \vec{k} \\ 0 & 0 & 1 \\ 1 & -1 & 1 \end{vmatrix} = \vec{i} + \vec{j} = \langle 1\,1\,0\rangle,$$

and $\overrightarrow{P_0P_1} = \langle 0\,0\,1\rangle \times \langle h\,\bar{k}\,l\rangle = \langle k\,h\,0\rangle$. The angle θ_1 between vectors $\overrightarrow{P_0A}$ and vector $\overrightarrow{P_0P_1}$ can be found by the inner product of these two vectors as $\overrightarrow{P_0A} \cdot \overrightarrow{P_0P_1} = |\overrightarrow{P_0A}||\overrightarrow{P_0P_1}| \cos\theta_1$. The angle between planes (1 $\bar{1}$ 0) and ($h\,\bar{k}$ 0), which is equal to θ_1, in terms of h and k is

$$\cos\theta_1 = \frac{h+k}{\sqrt{2}\sqrt{h^2+k^2}}. \tag{9}$$

The zone axis $\vec{L}$ of the two sidewalls (1 $\bar{1}$ 1) and (1 1 1) is

$$\vec{L} = \langle 1\,\bar{1}\,1\rangle \times \langle 1\,1\,1\rangle = -2\vec{i} + 0\vec{j} + 2\vec{k} = \langle \bar{2}\,0\,2\rangle. \tag{10}$$

Since the undercut plane is in the same zone as the sidewalls, it must be that $\langle h\,\bar{k}\,l\rangle \cdot \langle \bar{2}\,0\,2\rangle = 0$, or

$$h - l = 0. \tag{11}$$

The angle θ_1 can be obtained by measurement, we let $\sqrt{2}\cos\theta_1 = 1/\eta$, then equation (9) can be expressed in the form

$$(\eta^2 - 1)h^2 + 2\eta^2 hk + (\eta^2 - 1)k^2 = 0. \tag{12}$$

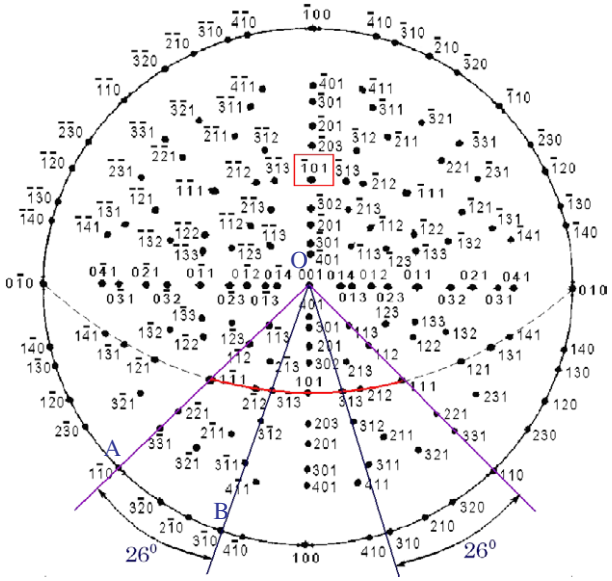

Figure 22. Location of the Miller indices of the {3 1 3} undercut plane in a ⟨0 0 1⟩ stereogram.

Solving (12) gives

$$h = \left\{ \frac{-2\eta^2 \pm \sqrt{4\eta^4 - 4(\eta^2-1)^2}}{2(\eta^2-1)} \right\} k = g(\eta)k. \tag{13}$$

Since $\theta_1 = 29°$, equation (13) gives $h = 3.487k$. Thus we have $h : k : l = 1 : g(\eta) : 1 = 3.487 : 1 : 3.487 \approx 7 : 2 : 7$.

In order to verify the Miller indices (7 $\bar{2}$ 7) of the undercut plane calculated on the assumption that undercut planes are of the same zone of the sidewalls, we perform an experiment which measures, by using the surface profiler, the angle between the undercut plane and the top (0 0 1) surface with the mask layer etched off. The probe of the surface profiler contacts the top surface and keeps going along the direction perpendicular to the edge $\overrightarrow{P_0P_1}$, over the edge it goes down the undercut plane. The angle β_e in figure 20 is measured to be $\tan^{-1}(57.44/53.31) = 47.13°$. The angle β_t between ⟨0 0 1⟩ and ⟨7 $\bar{2}$ 7⟩ is calculated as $\beta_t = \cos^{-1}(7/\sqrt{102}) = 46.12°$, which agrees well with β_e. Mayer [12] claimed the undercut

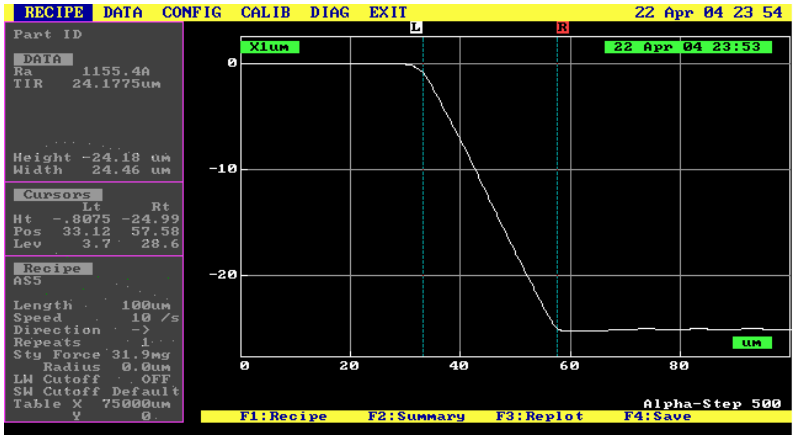

Figure 23. The angle between (0 0 1) and (3 1 3) is measured to be 44.67° by the surface profiler.

plane is (411), the angle between $\langle 0\,0\,1\rangle$ and $\langle 411\rangle$ is $\beta_t = \cos^{-1}(1/\sqrt{18}) = 76.37°$, which is far away from β_e. Let the angle between $\overrightarrow{P_0P_1}$ and $\overrightarrow{P_2P_1}$ be denoted by θ_3, we can further confirm our result by comparing the experimentally measured θ_3 with the theoretically calculated θ_3. Since $\overrightarrow{P_0P_1} = \langle 2\,7\,0\rangle$ and $\overrightarrow{P_2P_1} = \langle 7\,2\,7\rangle \times \langle 0\,0\,1\rangle = \langle 2\,\bar{7}\,0\rangle$, from the inner product of $\overrightarrow{P_0P_1}$ and $\overrightarrow{P_2P_1}$ we have $\theta_3 = \cos^{-1}(-45/53) = 148.1°$ which is very close to the measured value (= 148.5°as shown in figure 18). From the several verifications mentioned above, we know that the undercut planes are {7 2 7} and not {411} as mentioned by Mayer [12].

5.2. Aqueous KOH + IPA solutions

The proposed method for the Miller-index determination of the undercut surfaces can also be applied equally well to the case where the etching solution is KOH plus IPA. The angle between $\overrightarrow{S_0S_1}$ and $\overrightarrow{S_0A}$ in figure 21 is measured to be 26°. In figure 22 we draw a line $\overleftrightarrow{OB}$ at an angle of 26° with respect to the line $\overleftrightarrow{OA}$. Based on the assumption that the undercut plane belongs to the same zone as the sidewalls, the intersection of $\overleftrightarrow{OB}$ and the trace of the two {1 1 1} sidewalls gives the projected pole of the undercut plane. By using equation (8) the Miller indices of the undercut plane are calculated to be $(3\,\bar{1}\,3)$, which is of the {3 3 1} family. This result is the same as that of Bean [6]. The angle between (0 0 1) and $(3\,\bar{1}\,3)$ can then be calculated to be $\theta = \cos^{-1}(3/\sqrt{20}) = 46.5°$, which is very close to the angle 44.67° measured by the surface profiler (figure 23).

6. Conclusions

Although the undercutting behavior of a $Si_{(0\,0\,1)}$ convex corner had been widely studied, a sound theoretical background for the determination of the Miller indices of these undercut planes had not been found in the literature. In section 4 we have given a theoretical explanation for the emergence of undercut planes, and propose a 2D zoning model in which the undercut planes just beneath the mask layer are presumed to be in the same zone as the sidewalls forming the convex corner. Based on this model we have presented a method for determining the Miller indices of the undercut planes by using analytical geometry in conjugation with stereographic projection. The theoretical results have been verified by experimental angle measurement.

Acknowledgment

This paper was supported by the National Science Council of the Republic of China under the contract no NSC90-2212-E-002-15.

References

[1] Seidel H, Csepregi L, Heuberger A and Baumgärtel H 1990 Anisotropic etching of crystalline silicon in alkaline solutions *J. Electrochem. Soc.* **137** 3612–32

[2] Herr E and Baltes H 1991 KOH etch rates of high-index planes from mechanically prepared silicon crystals *Int. Conf. Solid-State Sensors and Actuators (San Francisco, CA)* pp 807–10

[3] Zielke D and Frühauf J 1995 Determination of rates for orientation-dependent etching *Sensors Actuators* A **48** 151–6

[4] Wiliams K R and Muller R S 1996 Etch rates for micromachining processing *J. Micro-electromech. Syst.* **5** 256–69

[5] Chen Chien-Tang, Tseng Fang-Churng, Chang Chun-Yen and Lee Ming-Kwang 1967 Study of electropic characteristics on thermally nitrided SiO_2 (nitroxide) films *J. Electrochem. Soc.* **114** 965

[6] Bean K E 1978 Anisotropic etching of silicon *IEEE Trans. Electron Devices* **25** 1185–94

[7] Bäcklund Y and Rosengren L 1992 New shapes in ⟨100⟩ Si using KOH and EDP etches *J. Micromech. Microeng.* **2** 75–9

[8] Baryeka I and Zubel I 1995 Silicon anisotropic etching in KOH–isopropanol etchant *Sensors Actuators* A **48** 229–38

[9] Kim B and Cho Dong-il Dan 1998 Aqueous KOH etching of silicon (1 1 0) *J. Electrochem. Soc.* **145** 2499–508

[10] Lee D B 1969 Anisotropic etching of silicon *J. Appl. Phys.* **40** 4569–74

[11] Abu-Zeid M M 1984 Corner undercutting in anisotropically etched isolation contours *J. Electrochem. Soc.* **131** 2138–42

[12] Mayer G K, Offereins H L, Sandmaier H and Kühl K 1990 Fabrication of non-underetched convex corners in anisotropic etching of (1 0 0) silicon in aqueous KOH with respect to novel micromechanic elements *J. Electrochem. Soc.* **137** 3947–3951

[13] Schröder H and Obermeier E 2000 A new model for $Si_{\{1\,0\,0\}}$ convex corner undercutting in anisotropic KOH etching *J. Micromech. Microeng.* **10** 163–70

[14] Zhang Q, Liu l and Li Z 1996 A new approach to convex corner compensation for anisotropic etching of (1 0 0) Si in KOH *Sensors Actuators* A **56** 251–4
[15] Bao M, Burrer C, Esteve J, Bausells J and Marco S 1993 Etching front of (1 1 0) strips for corner compensation *Sensors Actuators* A **37–38** 727–32
[16] Shaw D W 1979 Morphology analysis in localized crystal growth and dissolution *J. Cryst. Growth* **47** 509–17
[17] Shaw D W 1981 Localized GaAs etching with acidic hydrogen peroxide solutions *J. Electrochem. Soc.* **128** 874–80
[18] Séquin C H 1992 Computer simulation of anisotropic crystal etching *Sensors Actuators* A **34** 225–41
[19] Hubbard T J and Antonsson E K 1994 Emergent faces in crystal etching *J. Microelectro-mech. Syst.* **3** 19–28
[20] Danel J S and Delapierre G 1992 Anisotropic crystal etching: a simulation program *Sensors Actuators* A **31** 267–74
[21] Mckie D and Mckie C 1986 *Essentials of Crystallography* (Oxford: Blackwell)
[22] Kelly A, Groves G W and Kidd P 2000 *Crystallography and Crystal Defects* (NewYork: Wiley)
[23] Massalski B 1980 *Structure of Metals* 3rd edn (NewYork: McGraw-Hill)
[24] Royer D and Dieulesaint E 2000 *Elastic Waves in Solids I* (Berlin: Springer)